

## Optimal Design of Filament Wound Grid-stiffened Composite Cylindrical Structures

M. Buragohain\* and R. Velmurugan#

\*Advanced Systems Laboratory, Hyderabad-500 058

#Indian Institute of Technology Madras, Chennai-600 036

E-mail: buragohainm@yahoo.com, ramanv@iitm.ac.in

### ABSTRACT

An integral account of design and analysis of grid-stiffened cylindrical structures is presented. For convenience, a two-phase approach is adopted. In the initial phase, with a view to arriving at a few initial possible optimal configurations, parametric analysis through smeared stiffeners approach is utilised. The ribs, in a filament wound grid-stiffened structure, introduce several additional design elements that result in many possible design configurations; in the initial phase, these design options are efficiently reduced to a few numbers. Finite element modelling is used in the final design and analysis. Rib material is distinct from normal unidirectional composites and this aspect is inherently accounted for in the modelling approaches considered here.

**Keywords:** Filament winding, grid-stiffened shell, lattice cylinder, smeared stiffeners model, buckling

### NOMENCLATURE

$a, b, h$	Rib spacing, rib width and height respectively
$A, B, D$	Extensional stiffness matrix, extension-bending coupling stiffness matrix and bending stiffness matrix respectively
$A_{ij}, B_{ij}, D_{ij}$	Elements of stiffness matrices
$A_{ij}^*, B_{ij}^*, D_{ij}^*$	Elements of compliance matrices
$h_k$	$z$ coordinate of the $k_{th}$ ply
$M_x, M_y, M_{xy}$	Moments per unit length applied on the grid of stiffening ribs
$M_{xequ}, M_{yequ}, M_{xyequ}$	Moments per unit length of the equivalent shell
$n$	Number of plies
$n_a, n_c, n_h$	Number of axial, circumferential and helical ribs respectively
$N_h$	Number of starts
$N, M$	Vectors of unit in-plane forces and moments respectively for the ribs/skins
$N_x, N_y, N_{xy}$	In-plane forces per unit length applied on the system of stiffening members
$N_{xequ}, N_{yequ}, N_{xyequ}$	In-plane forces per unit length of the equivalent shell
$t$	Skin thickness
$\bar{Q}_{ij}^k$	Elements of reduced transformed stiffness matrix of the $k_{th}$ ply of the composite laminate making the ribs/skins

$U$	Strain energy of the shell
$U_{P_xrib}, U_{P_xhco}, U_{P_xcco}$	Strain energies of the rib segments, helical-to-helical cross-overs and circumferential-to-helical crossovers respectively under an axial compressive force of $P_x$
$x, y, z$	Axial, circumferential and radial coordinates as per cylindrical coordinate system
$\alpha$	Helical angle
$\varepsilon_x^0, \varepsilon_y^0, \gamma_{xy}^0$	In-plane normal and shear strains in the mid-plane
$\varepsilon_x^1, \varepsilon_y^1, \gamma_{xy}^1$	Changes in curvatures in the mid-plane
$\varepsilon^0, \varepsilon^1$	Vectors of in-plane strains and changes in curvatures respectively
$\Delta$	Surface area

### 1. INTRODUCTION

Filament wound grid-stiffened composite cylindrical structures are consistently gaining acceptance and popularity in many aerospace and other high-end applications that demand reliability and mass efficiency. The grid of stiffening ribs that are made by filament winding makes such a structure very highly efficient and reliable. Mass efficiency and reliability of these structures are derived mainly from the unidirectional nature of the ribs. An optimal grid-stiffened structure has only a grid of stiffening ribs without any skin<sup>1</sup>. However, depending upon functional requirements, an outer skin (and occasionally an inner one as well) is provided. Very often such a structure is subjected to axial

compression wherein buckling behaviour is of critical importance. These structures are known for a special characteristic, normally referred to as self-stabilisation, that makes these largely immune to manufacturing and testing imperfection and very high specific buckling load-carrying capacity is obtained. The essential feature of these structures is the presence of a grid of ribs that are basically unidirectional composites but with a distinct difference from normal unidirectional composites. The ribs that are either helical or circumferential or axial or a combination thereof are made by filament winding. Different types of lattice patterns comprising triangles, hexagons, and diamonds can be formed by choosing suitable types of ribs and their relative locations. Due to the continuous nature of filament-winding process, the fibres of one rib cross over the fibres of other ribs at certain nodal points/zones (would refer to these zones as crossovers) such that effective thickness of the crossovers is more than that in the rib segments. As a result, variation of material properties is found from the crossovers to the rib segments.

An integrated note on design and analysis, manufacture and testing of grid-stiffened composite shell is given by Vasiliev<sup>1,2</sup> *et al.* Initial design/analysis is based on a continuum model where stiffening ribs are smeared to arrive at an equivalent shell. Smeared stiffeners approach is based on mathematical models that smear the stiffening ribs into an equivalent ply. This approach is especially useful in global buckling analysis in the initial design phase. As a concept, smearing of stiffeners is not new, especially in stiffened metallic shells. For composites, several smeared stiffeners models were presented in the recent past<sup>3-11</sup>. Different criteria such as rib spacing, stiffness contribution (by force-moment analysis), equivalence of strain energy, etc. have been adopted for smearing the stiffeners. While transverse strain and shear strains are neglected by some authors, a smeared stiffeners model that accounts for transverse shear flexibility is used by Jaunky<sup>8,9</sup> *et al.* and Damodar<sup>10</sup> *et al.* In another approach, stiffness matrix of the equivalent shell is obtained by smearing the ribs based on spacing, whereas, the final analysis is done by finite element modelling<sup>11</sup>.

Due to the presence of numerous possibilities in terms of design parameters, smeared stiffeners approach is more efficient in the initial design phase, especially by means of a parametric analysis, to narrow down design options. However, finite element modelling is more popular in the final phase of design.

While several authors have worked on design and analysis, manufacture and testing of grid-stiffened composite structures, work that has considered material property variation from crossover locations to ribs, is rare. Vasiliev<sup>1</sup> *et al.* have made a mention of this aspect of lattice structures. Material properties of the ribs are determined from specimens cut from actual components and estimates are revised. Velmurugan<sup>12</sup>, *et al.* have introduced the concept and devised specimens for mechanical characterisation of rib unidirectional composites. Smeared stiffeners model presented by Buragohain<sup>5</sup>, *et al.* takes this variation in material properties into account.

In this paper, an integrated account of design and analysis of grid-stiffened cylindrical structures under axial compression is presented. Design and analysis has been broadly divided into two phases-initial phase and final phase. In the initial phase of design, parametric analysis through smeared-stiffeners approach is adopted to arrive at an optimal configuration. Finite element modelling is used in the final phase of design.

## 2. DESIGN AND ANALYSIS

Various parameters (Fig. 1) associated with a cylindrical grid-stiffened structure can be listed as: length  $L$ , radius  $R$ , type of lattice pattern, height of stiffening ribs  $h$ , width of stiffening rib  $b$ , orientation of helical ribs  $\alpha$ , number of stiffening ribs, distance between stiffening ribs  $a$  and thickness  $t$  and ply sequence of skin, etc. Given the length and radius of the structure, an optimal design exercise is essentially that of determining the design parameters that would resist the design load with desired factor of safety and minimum mass. For a cylinder of radius  $R$  under both axial compression  $F$  and bending moment  $M$ , the design load  $P$  is taken as

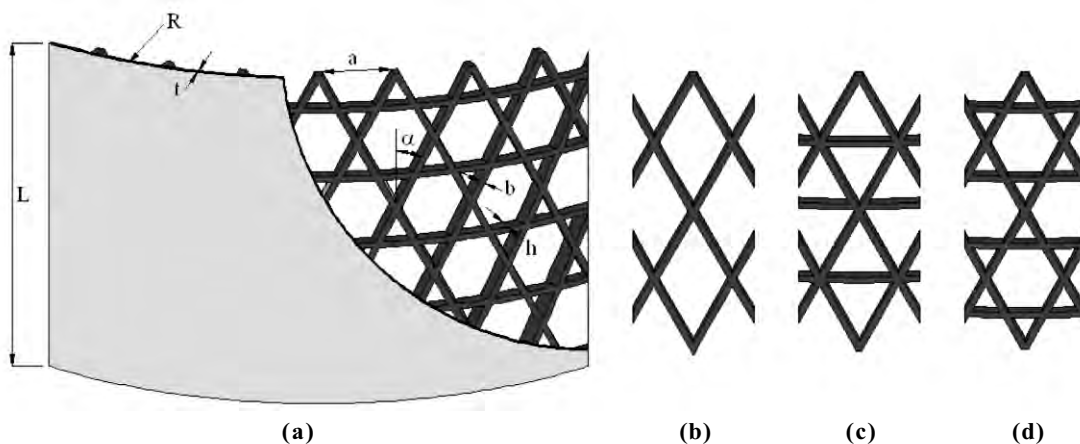


**Figure 1. Design parameters: (a) panel of a grid-stiffened cylinder, (b), (c), (d) lattice patterns –diamond, triangular and hexagonal respectively.**

$$P = F + \frac{2M}{R} \quad (1)$$

Under such a loading condition, strength failure and buckling are identified as the two broad likely failure modes. Buckling may take place in three different ways: global buckling, rib crippling, and local skin buckling. For an optimal design, in the initial phase of design, one would attempt to have global buckling. (Stress failure criterion can be applied in the final phase.) Analysis tools such as finite element modelling (FEM) can be employed for both buckling analysis as well as stress analysis. However, due to the presence of so many design parameters, as indicated above, FEM is not efficient in the initial phase of design.

## 2.1 Smearred Stiffeners Model

Smearred stiffeners model (SSM)-based approach is a very simple and efficient tool and it is useful in the initial phase of design and analysis of a lattice structure. Different criteria, such as equality of cross-sectional area, equality of strain energy, etc can be applied to smear the stiffening ribs so as to obtain an equivalent shell. In this model, strain energy of the equivalent shell is equated to that of the grid of stiffening ribs. Analytical formulations following classical laminate plate/shell theory are conveniently used in this process. The linear constitutive relations can be expressed as:

$$\begin{Bmatrix} \mathbf{N} \\ \mathbf{M} \end{Bmatrix} = \begin{bmatrix} \mathbf{A} & \mathbf{B} \\ \mathbf{B} & \mathbf{D} \end{bmatrix} \begin{Bmatrix} \boldsymbol{\varepsilon}^0 \\ \boldsymbol{\varepsilon}^1 \end{Bmatrix} \quad (2)$$

The vectors and matrices in Eqn (2) are defined as

$$\{\mathbf{N}\} = \begin{Bmatrix} N_x \\ N_y \\ N_{xy} \end{Bmatrix} \quad \text{and} \quad \{\mathbf{M}\} = \begin{Bmatrix} M_x \\ M_y \\ M_{xy} \end{Bmatrix} \quad (3)$$

$$A_{ij} = \sum_{k=1}^n \bar{Q}_{ij}^k (h_k - h_{k-1})$$

$$B_{ij} = \frac{1}{2} \sum_{k=1}^n \bar{Q}_{ij}^k (h_k^2 - h_{k-1}^2) \quad (4)$$

$$D_{ij} = \frac{1}{3} \sum_{k=1}^n \bar{Q}_{ij}^k (h_k^3 - h_{k-1}^3)$$

$$\{\boldsymbol{\varepsilon}^0\} = \begin{Bmatrix} \varepsilon_x^0 \\ \varepsilon_y^0 \\ \gamma_{xy}^0 \end{Bmatrix} \quad \text{and} \quad \{\boldsymbol{\varepsilon}^1\} = \begin{Bmatrix} \varepsilon_x^1 \\ \varepsilon_y^1 \\ \gamma_{xy}^1 \end{Bmatrix} \quad (5)$$

Equation (2) is used to express the strains in terms of force/moment resultants and compliance matrix elements and the following expression for strain energy of an orthotropic cylindrical shell is obtained as

$$U = \frac{\Delta}{2} \left[ \begin{aligned} & \left( A_{11}^* N_x^2 + A_{22}^* N_y^2 + A_{66}^* N_{xy}^2 \right) \\ & + 2 \left( A_{12}^* N_x N_y + A_{16}^* N_x N_{xy} + A_{26}^* N_y N_{xy} \right) \\ & + 2 \left( B_{11}^* N_x M_x + B_{22}^* N_y M_y + B_{66}^* N_{xy} M_{xy} \right) \\ & + 2 \left( B_{12}^* N_x M_y + B_{21}^* N_y M_x + B_{16}^* N_x M_{xy} \right) \\ & + 2 \left( B_{61}^* N_{xy} M_x + B_{26}^* N_y M_{xy} + B_{62}^* N_{xy} M_y \right) \\ & + \left( D_{11}^* M_x^2 + D_{22}^* M_y^2 + D_{66}^* M_{xy}^2 \right) \\ & + 2 \left( D_{12}^* M_x M_y + D_{16}^* M_x M_{xy} + D_{26}^* M_y M_{xy} \right) \end{aligned} \right] \quad (6)$$

A smeared stiffeners model is developed adopting two different smearing approaches - (i) discrete stiffeners approach<sup>4</sup> and (ii) unit cell approach<sup>5</sup>. Equation (6) contains twenty one terms each of which corresponds to a compliance matrix element and certain force/moment resultant(s). The strain energy expression for the equivalent shell is made to contain only one unknown compliance matrix element by considering different non-zero load cases. Thus, 21 different non-zero load cases, each corresponding to a compliance matrix element, are applied in Eqn (6) such that in each case the strain energy of the equivalent shell is expressed in terms of an unknown compliance matrix element. In the discrete stiffeners approach the grid of stiffening ribs is considered as a collection of discrete ribs. Geometrical details of the lattice structure are used and ratios of force/moment resultants are expressed as follows:

$$\frac{N_x}{N_{xequ}} = \frac{M_x}{M_{xequ}} = \frac{2\pi R \cos \alpha}{b(2n_h + n_a \cos \alpha)}$$

$$\frac{N_y}{N_{yequ}} = \frac{M_y}{M_{yequ}} = \frac{2\pi R \sin \alpha}{b(2n_h + n_c \sin \alpha)} \quad (7)$$

$$\frac{N_{xy}}{N_{xyequ}} = \frac{M_{xy}}{M_{xyequ}} = \frac{2\pi R \cos \alpha}{b(2n_h + n_a \cos \alpha)}$$

Under each load case, strain energy of the grid of ribs is equated to that of the equivalent shell and an element of the equivalent compliance matrix is obtained. Stiffness matrix of the equivalent shell is obtained by inverting the compliance matrix and the final buckling load is estimated by employing Ritz buckling analysis procedure. This is an extremely quick and versatile model as it can consider virtually any lattice pattern that involves any combination of stiffening ribs—helical, circumferential or axial.

Although the stiffening ribs are unidirectional in nature, material properties at the ribs are different from crossover material properties. Experiments carried out on specially devised specimens that simulate rib material properties have shown that longitudinal modulus of carbon unidirectional composites at the rib portion can be as low as 53 per cent of that of normal unidirectional carbon composites<sup>12</sup>. Difference in material properties in the rib segments to crossovers

is primarily on account of the presence of alternating resin rich layers in the rib segments, especially near the crossovers. Transverse and in-plane shear properties of rib unidirectional composites are also affected although to different extents. To take these differences into account, for better accuracy, the unit cell approach is developed. A unit cell that represents the grid of stiffening ribs is considered (Fig. 2). For large number of plies, as is the likely case in practice, the crossovers tend to become symmetric and so  $B_{ij}^* = 0$ . Further, derivations in terms of strain energies, lead to  $A_{16}^* = A_{26}^* = D_{16}^* = D_{26}^* = 0$ . Thus, from Eqn (6), for the equivalent shell, the number

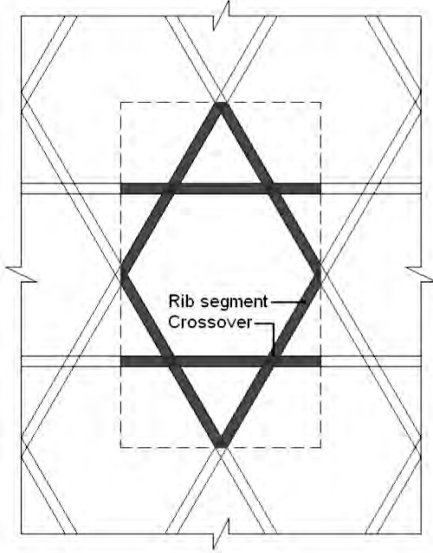


Figure 2. Typical unit cell.

of non-zero load cases is reduced to eight. These are: (i)  $N_{xequ} \neq 0$ , (ii)  $M_{xequ} \neq 0$ , (iii)  $N_{yequ} \neq 0$ , (iv)  $M_{yequ} \neq 0$ , (v)  $N_{xyequ} \neq 0$ , (vi)  $M_{xyequ} \neq 0$ , (vii)  $N_{xequ} \neq 0$  &  $N_{yequ} \neq 0$  and (viii)  $M_{xequ} \neq 0$  &  $M_{yequ} \neq 0$ . (In each of the above load cases, all the stress resultants except the specified ones are zero.) Strain energy expression for the equivalent shell under each load case would contain only one unknown compliance matrix element. The load cases considered in the strain energy formulations of the equivalent shell are also considered in the strain energy formulations of the stiffening ribs. Identical loads are applied in each load case with one difference in the way that instead of distributing a force continuously over a length, here a force is discretely distributed in the ribs and force/moment distribution is found out. The compliance matrix elements of the rib segments and crossovers, along with the force/moment distribution, are used to obtain the strain energy expressions of the lattice cylinder under each load case. Thus, for example, for a lattice pattern of triangles and hexagons made by helical and circumferential ribs, the final strain energy expressions for the rib segments, helical-to-helical crossovers and circumferential-to-helical crossovers under the first load case, i.e.  $N_{xequ} \neq 0$ , simulated by an axial compressive force  $P_x$ , are given as follows:

$$U_{P_x,rib} = \frac{LA_{11rib}^* P_x^2}{4\pi R b \cos^3 \alpha} \left[ \frac{\pi R}{N_h} (1 + \sin^3 \alpha) - \frac{b}{2 \cos \alpha} (1 + 2 \sin \alpha + 2 \sin^3 \alpha) \right]$$

$$U_{P_x,hco} = \frac{LP_x^2}{4\pi R \cos^4 \alpha} (A_{11hco}^* \cos^4 \alpha + A_{22hco}^* \sin^4 \alpha + 2A_{12hco}^* \cos^2 \alpha \sin^2 \alpha)$$

$$U_{P_x,cco} = \frac{LP_x^2 A_{11cco}^* \sin \alpha}{4\pi R}$$
(8)

Strain energy of the lattice cylinder under  $P_x$  is

$$U_{P_x} = U_{P_x,rib} + U_{P_x,hco} + U_{P_x,cco}$$
(9)

And, equating the strain energies, we get

$$A_{11equ}^* = \frac{2U_{P_x}}{\Delta_{equ} N_{xequ}^2}$$
(10)

Thus, one element of the equivalent compliance matrices is obtained from one load case. Similar strain energy expressions for other load cases are also found and corresponding compliance matrix elements are obtained. In this procedure of smearing the stiffening ribs into an equivalent shell, laminate stiffness matrices (**A**, **B** & **D** matrices) for crossover locations and ribs are found out separately and thus, material property variation from crossover location to rib is taken care of. Once again, elements of the stiffness matrix of the equivalent shell are used in Ritz buckling analysis procedure by minimising potential energy of the equivalent shell.

## 2.2 Parametric Analysis

In a typical design exercise, initially, parametric analysis is carried out using smeared stiffeners models described above to narrow down design variables. As an example, a cylindrical structure of nominal diameter of 140 mm and overall length of 200 mm is taken. The loads acting on it are an axial force of 20 kN and bending moment of 2 kN-m. Using Eqn (1), these loads are readily converted to an equivalent axial force of 77.1 kN. Standard ASTM specimens for normal unidirectional carbon/epoxy composites and specially designed specimens for rib unidirectional composites were made and tested<sup>12</sup>. Material properties used are as follows:  $E_{11} = 83.3$  GPa,  $E_{22} = 6.9$  GPa,  $G_{12} = 4.9$  GPa, and  $\nu_{12} = 0.289$  for normal unidirectional composites and  $E_{11} = 44.2$  GPa,  $E_{22} = 5.0$  GPa,  $G_{12} = 2.4$  GPa, and  $\nu_{12} = 0.194$  for rib unidirectional composites, respectively.

Given the nominal diameter and length of the cylindrical structure and the design axial compressive force, the first step is to choose an appropriate lattice pattern. Several lattice patterns can be formed using: (i) helical ribs only, (ii) helical and circumferential ribs, and (iii) helical and axial ribs and effect of helical angle on buckling load is dependent on these lattice patterns. A wide spectrum of sizes (radius and length) and other features such as  $L/D$  ratio,  $h/b$  ratio, etc have been considered and a typical plot showing the effect of helical angle on buckling load

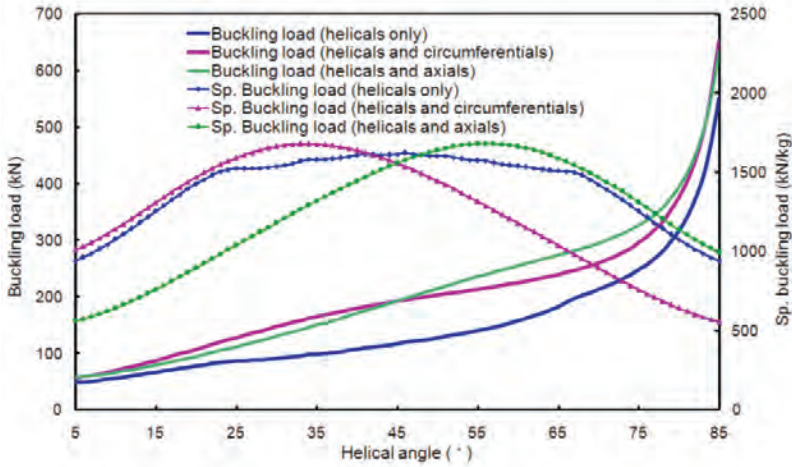


Figure 3. Effect of helical angle on buckling load and specific buckling load of a lattice cylinder of  $R = 70$  mm,  $L = 200$  mm,  $b = 6$  mm,  $h = 3$  mm and  $N_h = 6$ .

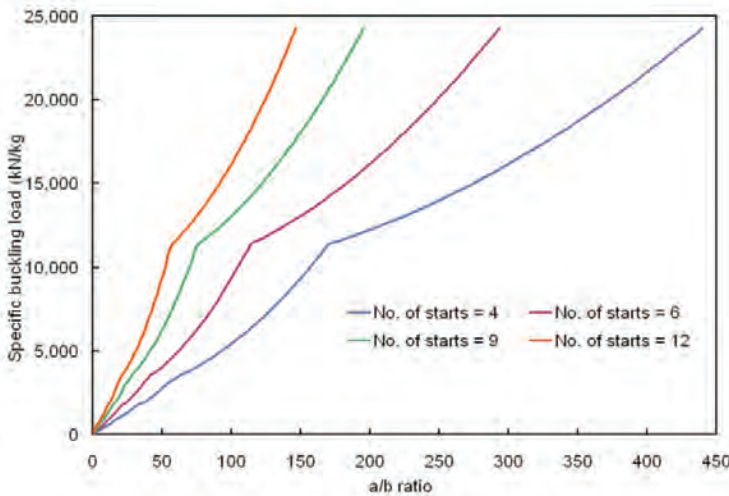


Figure 4. Effect of  $a/b$  ratio on specific buckling load of a lattice cylinder of  $R = 70$  mm,  $L = 200$  mm,  $b \times h = 18$  mm<sup>2</sup>.

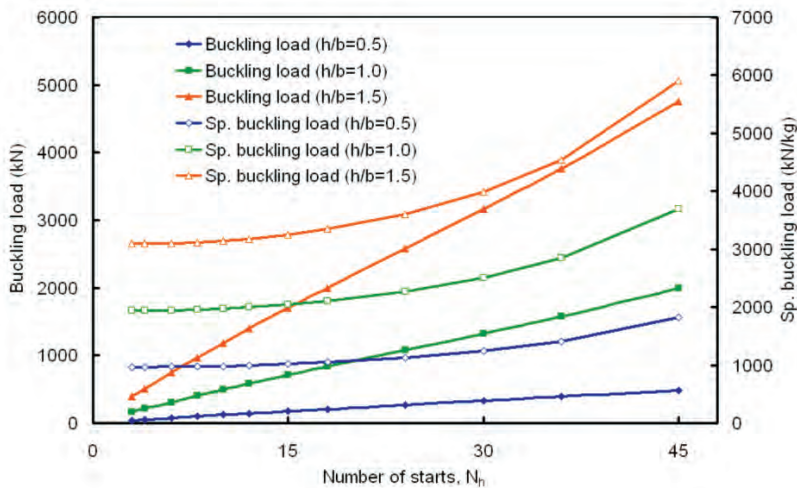


Figure 5. Effect of number of starts on buckling load and specific buckling load of a lattice cylinder of  $R = 70$  mm,  $L = 200$  mm,  $b = 6$  mm.

is given in Fig. 3. Buckling load increases with increasing helical angle and irrespective of the lattice pattern, it is very high for high helical angle. But, at high helical angles, the helical ribs tend to overlap each other and such configurations are not practicable. Also, specific buckling loads are rather low at high (as well as low) helical angles. It is found that optimal helical angle, depending upon the lattice pattern, lies between  $30^\circ$  to  $60^\circ$ . For the case of stiffening grid with helical ribs alone, optimal helical angle is around  $45^\circ$  whereas for stiffening grids with helical with circumferential ribs and helical with axial ribs, optimal helical angle is around  $30^\circ$  and  $60^\circ$ , respectively. As indicated by the specific buckling loads for the three different lattice patterns, for most of the range of helical angles, stiffening grids of helical ribs together with either circumferential ribs or axial ribs are more efficient than helical ribs alone. At high helical angles, axial ribs are better than circumferential ribs, but from manufacturing point of view, axial ribs are suitable for doubly curved structures and, for cylindrical structures circumferential ribs are more convenient. Thus, for our given example, a lattice pattern of triangles and hexagons with helical and circumferential ribs is chosen. Helical angle chosen is  $30^\circ$ .

Effect of ratio of rib spacing-to-rib width ( $a/b$  ratio) on specific buckling load of a lattice cylinder is shown Fig. 4. For a given number of starts (i.e., number of pairs of helical ribs), at a constant rib cross-sectional area,  $a/b$  ratio is increased by reducing the width of the ribs and increasing the rib thickness. It can be seen that increased  $a/b$  ratio at constant rib cross-sectional area would mean increased stiffness for the same mass. As a result, it is seen that the specific buckling load increases with increasing  $a/b$  ratio. It also implies that, for a given cross-sectional area of ribs, specific buckling load increases with increasing depth of ribs. In a strict sense, for a given number of starts, the rib spacing remains constant. Effect of number of starts on buckling load and specific buckling load of a lattice cylinder for different  $h/b$  ratio is shown in Fig. 5.

With increasing number of starts, for a given rib cross-section, total rib cross-sectional area of the lattice structure increases and the buckling load increases. Effect of number of starts on specific buckling load, however, is very marginal, especially for lower number of starts. As a result, a dense system of stiffening ribs of lower width but higher depth is theoretically preferable. This is especially true with large size structures. However, in a small lattice structure, such as the one in this case study, certain aspects of fabrication, such as relative size of groove cutting tool, vis-à-vis, circumferential dimension of the cylinder, etc play a more dominant

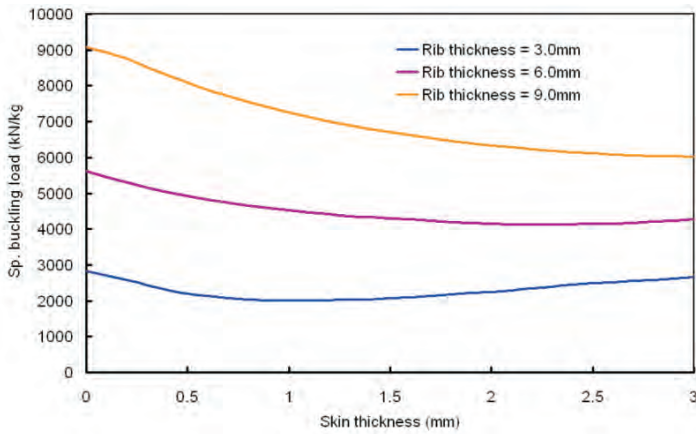


Figure 6. Effect of skin thickness on specific buckling load of lattice cylinder of  $R = 70$  mm,  $L = 200$  mm and  $b = 6$  mm.

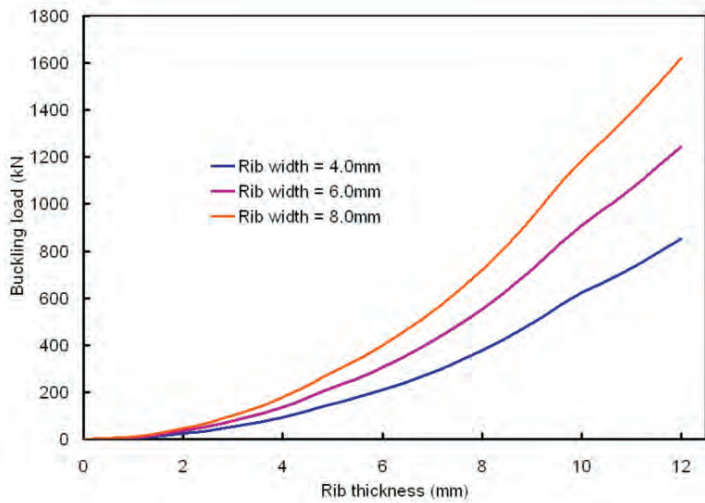


Figure 7. Variation of buckling load (as per SSM) with rib thickness for a lattice cylinder of  $R = 70$  mm,  $L = 200$  mm and  $N_h = 6$ .

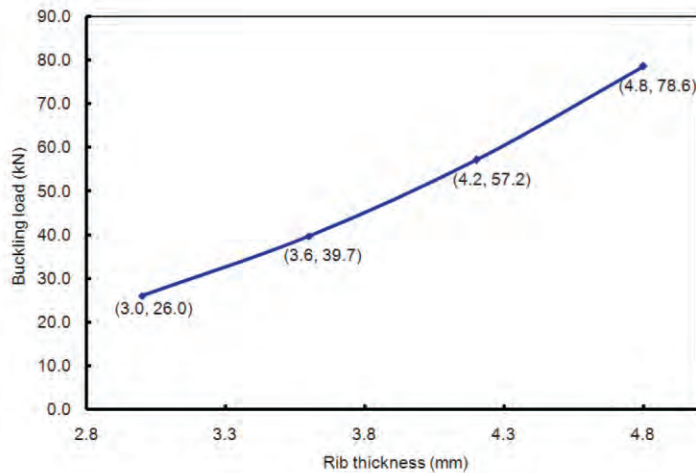


Figure 8. Variation of buckling load (as per FEM) with rib thickness for a lattice cylinder of  $R = 70$  mm,  $L = 200$  mm,  $b = 6$  mm and  $N_h = 6$ .

role in choosing the rib dimensions and rib density. Accordingly, a 6-start helical pattern with ribs of width 6 mm is chosen.

In a grid-stiffened shell under axial compression, gross cross-sectional area (thus, stiffness) increases as the skin thickness is increased. It can be expected that the buckling load will also increase. However, changes in specific buckling load would depend upon relative changes in buckling load and mass of the shell. In a grid-stiffened shell the ribs are the predominant structural elements and the rib thickness is much higher than the skin thickness. For such high rib thickness cases ( $t/h \leq 0.5$ , approx.), the skin primarily adds to the weight without any significant contribution to the overall stiffness and the specific buckling load decreases. Specific buckling load of a lattice cylinder initially decreases with skin thickness (Fig. 6). Thus, a lattice structure (without any skin) under axial compression is an optimal structure with specific buckling load as the criterion and in our case study also no skin is provided.

Figure 7 shows variation of buckling load of the cylinder with rib depth; the depth of rib corresponding to the equivalent axial force is 3 mm. However, for a small structure with a very few numbers of ribs, smeared stiffeners model is likely to overestimate the buckling load of the cylinder. Thus, rib thickness arrived at based on smeared stiffeners model may rather be considered as a lower bound.

### 2.3 Finite Element Modelling

Modelling of the stiffening ribs is the key to efficient modelling of a grid-stiffened structure. General purpose finite element package ANSYS is used for modelling and analysis<sup>13</sup>. While different types of elements, under the broad groups, viz., beam, shell and brick, can be used, use of 3-dimensional layered brick elements with 20 nodes for Modelling the stiffening ribs gives reliable estimates of buckling load. Modelling of the ribs is started by creating the nodes of a repeating unit. Elements are created by joining the nodes in such a way as to align the fibres in the rib direction. Overall model of the cylinder is developed by copying this building block. Different data tables are used for the ribs, helical-to-helical crossover locations and helical-to-circumferential crossover locations such that material properties and fiber orientations are duly represented. Thus, rib segments are modelled as unidirectional laminate with rib unidirectional composite properties and the crossovers are modelled

as angle-ply laminate of  $[+\alpha/-\alpha]_n$ ,  $[+\alpha/90^\circ]_n$  or

$[-\alpha/90^\circ]_n$  ply construction with normal unidirectional

composite properties. Boundary conditions applied are as follows:

- At the bottom of the cylinder axial, circumferential

and radial displacements are equal to zero and at the top of the cylinder circumferential and radial displacements are equal to zero.

- Further, the axial displacements of the nodes at the top of the cylinder are coupled.
- Axial compressive force, if applied at the top of the cylinder, and linear buckling analysis is carried out in two steps. In the first step the pre-buckling stresses of the cylinder are obtained by a static solution run of the model. In the second step an eigenvalue problem is solved wherein 'Block Lanczos' method is adopted to extract the eigenvalues and the critical buckling load is determined.

Finite element modelling is appropriate for the final analysis of the grid-stiffened structure. Parametric analysis based initial design reduces the possible parameters drastically and finite element analysis is carried out on a limited number of feasible configurations. Thus, continuing with our example given in the section on parametric analysis, it is found that these configurations vary only in respect of rib thickness (Fig. 8).

### 3. CONCLUSION

An integral account of design and analysis of grid-stiffened composite cylinder is given. Smear stiffeners approach is useful and efficient in the initial design phase, especially by way of parametric analysis, to narrow down design parameters so that overall configuration of the cylinder is determined. It is found that structurally, with specific buckling load as the criterion, a lattice cylinder with high rib thickness and without any skin is optimal. The grid should preferably contain, in addition to helical ribs, either circumferential or axial ribs. The orientation of the helical ribs, for an optimal structure, depends on the lattice pattern and, in general, it is between 30° to 60°. In the final phase of design, finite element analysis is more reliable as it can cater to local details as well. In both the cases, it is necessary to distinguish rib unidirectional composite from normal unidirectional composite material.

### REFERENCES

1. Vasiliev, V.V.; Barynin, V.A. & Rasin, A.F. Anisogrid lattice structures - survey of development and application. *Composite Structures*, 2001, **54**, 361-70.
2. Vasiliev, V.V. & Rasin, A.F. Anisogrid composite lattice structures for spacecraft and aircraft applications. *Composite Structures* 2006, **76**, 182-89.
3. Jones, R.M. Buckling of circular cylindrical shells with multiple orthotropic layers and eccentric stiffeners. *AIAA Journal*, 1968, **6**(12), 2301-305.
4. Velmurugan, R. & Buragohain, M. Buckling analysis of grid-stiffened composite cylindrical shell. *Journal of Aerospace Sciences and Technologies*, 2007, **59**(4), 282-93.
5. Buragohain, M. & Velmurugan, R. Buckling analysis of composite hexagonal lattice cylindrical shell using smeared stiffener model. *Def. Sci. J.*, 2009, **59**(3), 230-238.
6. Wodesenbet, E.; Kidane, S. & Pang, S. Optimization for buckling loads of grid stiffened composite panels. *Composite Structures*, 2003, **60**, 159-69.
7. Kidane, S.; Li, G.; Helms, J.; Pang, S. & Woldesenbet, E. Buckling load analysis of grid stiffened composite cylinders. *Composites Part B: Engineering*, 2003, **34**, 1-9.
8. Jaunky, N.; Knight, N.F. & Damodar, R.A. Formulation of an improved smeared stiffener theory for buckling analysis of grid-stiffened composite panels. *Composites Part B: Engineering*, 1996, **27B**, 519-26.
9. Jaunky, N. & Knight, N.F. Optimal design of grid-stiffened composite panels using global and local buckling analyses. *Journal of Aircraft*, 1998, **35**, 478-86.
10. Damodar, R.A. and Jaunky, N. Optimal Design of Grid-Stiffened Panels and Shells with Variable Curvature. *Composite Structures*, 2001, **52**, 173-180.
11. Slinchenko, D. and Verijenko, V.E. Structural analysis of composite lattice shells of revolution on the basis of smearing stiffness. *Composite Structures*, 2001, **54**, 341-48.
12. Velmurugan, R. and Buragohain, M. Rib UD Composites for Grid-stiffened Composite Shell. *In Proceedings of the ISAMPE National Conference on Composites INCCOM-7*, 4-5 December 2008, Bengaluru, 377-85.
13. ANSYS Theory Reference (ANSYS 10.0 Users Manual).

### Contributors



**Dr Manojkumar Buragohain** obtained MTech from IIT Madras in 1992 and PGDFA (CFA) from ICAI Hyderabad in 2000. He has done PhD from IIT Madras in 2010. Presently he is working as Scientist 'F' at Advanced Systems Laboratory, Hyderabad. His areas of interest include: Geodesic and non-geodesic filament winding of axisymmetric as well as non-axisymmetric components, tape winding, rosette lay-up and contact lay-up. He has worked for design and development of composite motor casing, grid-stiffened structures, ablative liners, wind mill blade, etc.



**Dr R Velmurugan** is presently a Professor at the Composites Technology Centre, Department of Aerospace Engineering, IIT Madras, Chennai. He has about 15 years of teaching and research experience. He has guided many students for PhD/MS/MTech degree programmes. His areas of interest include: Impact mechanics, structural crashworthiness and nano composites.